

PERIODIC VARIABILITY FROM THE 2MASS CALIBRATION SCANS

JAMES R. A. DAVENPORT^{1,2}, ANDREW C. BECKER², PETER PLAVCHAN³, ROC CUTRI³
Draft version March 27, 2014

ABSTRACT

We report on a systematic search through the 2MASS Calibration Point Source Working Database for systems exhibiting periodic variability. While the total areal coverage of the data is modest, the temporal coverage is significant, with more than 100 million 3-band photometric measurements of 113,030 point sources. Our sample represents the most complete compendium of periodic variability in the near-infrared. Our data mining efforts recovered **XXX** periodic systems, which include **XXX** eclipsing binary systems and **XXX** radial pulsators – **XXX** RR Lyrae Type ab, **XXX** RR Lyrae Type c, **XXX** Cepheids, and one short-period δ Scuti star. Hysteresis in the color–color evolution of these pulsating systems provides valuable insights into the underlying stellar astrophysics. Our search also recovered **XXX** quasi-periodic long-period variables, which vary on a characteristic timescale, but whose lightcurves are not repeatable cycle to cycle. We examine particularly rich variable star fields including those in ρ Ophiuchus, and in the Small and Large Magellanic Clouds. We outline principles for multi-band periodic variable star classification using periods and multi-band amplitudes and skews. This will prove to be a benchmark reference sample until large area, near-IR time-domain surveys become a reality.

This includes an initial investigation of the relative importance of near-IR lightcurve attributes for classification purposes.

Subject headings: variability, surveys, NIR

1. INTRODUCTION

Arguably the two greatest advancements in optical and infrared photometric surveys within the past two decades have been the advent of 1% accurate multi-wavelength photometry for contiguous portions of the sky exceeding $\Omega \sim 10^4$ deg² (e.g. Skrutskie et al. 2006; Wright et al. 2010; Aihara et al. 2011), and time resolved surveys spanning baselines of days to years (e.g. Ivezić et al. 2007; Sesar et al. 2011). As both the temporal and spatial domains are explored, new astrophysical phenomena are uncovered, while previously rare events are placed in a statistical context. Naturally, next generation surveys will exploit both of these domains simultaneously, producing deep multi-wavelength surveys with both unprecedented spatial and temporal coverage (Kaiser et al. 2002; Ivezić et al. 2008). In order to prepare for these future surveys, which will contain orders of magnitude larger numbers of variable sources, existing catalogs and databases provide valuable insights into the data complexity, and serve as testing grounds for identification and classification of phenomena. Such studies will precipitate the development of new techniques, which in turn may inform the targeting, cadence, and observing strategies of the future surveys (e.g. Oluseyi et al. 2012).

The Two Micron All Sky Survey (2MASS; Skrutskie et al. 2006) imaged the full sky in three, simultaneously obtained, near-infrared (NIR) bands. Survey operations were conducted between 1997 and 2001, using a northern and southern telescope. Photometric calibration for 2MASS was accomplished using repeated observations

of 35 selected fields, which were spaced across the sky (Nikolaev et al. 2000). An additional 5 tiles were imaged around the Large and Small Magellanic Clouds during the last year of operation. Each calibration field covered an area of approximately 8.5' (RA) \times 1° (Dec). The 35 standard calibration fields were scanned ranging between 562 and 3,692 times over the 4 year period, yielding some of the most densely sampled and well-calibrated NIR light curves yet produced. The placement of these tiles is shown in Figure 1, and they contain light curves for approximately 110,000 point source objects. These data were released as part of the 2MASS Extended Mission (Cutri 2006), and collectively define the 2MASS Calibration Point Source Working Database (Cal-PSWDB).

This unique dataset has been used for a handful of studies to date. Plavchan et al. (2008b) characterized many of the details in analyzing this unique dataset for time domain studies. They also mined these data for periodic objects, finding 3 new M dwarf eclipsing binaries. Plavchan et al. (2008a) studied the 131 day periodic object, 2MASS J16271848–2429059, revealing a possible three-body YSO system. Sarajedini et al. (2009) utilized the images from multiple scans of calibration tile 90067 to produce a NIR color-magnitude diagram for the open cluster M67 that probed $\gtrsim 3$ magnitudes deeper than the standard 2MASS point source catalog. Becker et al. (2008) discovered and characterized a 2.6-day periodic M dwarf binary, 2MASS J01542930+0053266. This system was located in both the 2MASS calibration tile 90004, and the “Stripe 82” region of the Sloan Digital Sky Survey footprint, which yielded an 8-band light curve ($ugrizJHK_s$) for the binary. Using 16 of the calibration tiles that overlapped the SDSS footprint, Davenport et al. (2012) produced some of the first constraints on the properties of M dwarf flares in red optical and NIR

¹ Corresponding author: jrad@astro.washington.edu

² Department of Astronomy, University of Washington, Box 351580, Seattle, WA 98195

³ Infrared Processing and Analysis Center, California Institute of Technology, Pasadena, CA 91125, USA

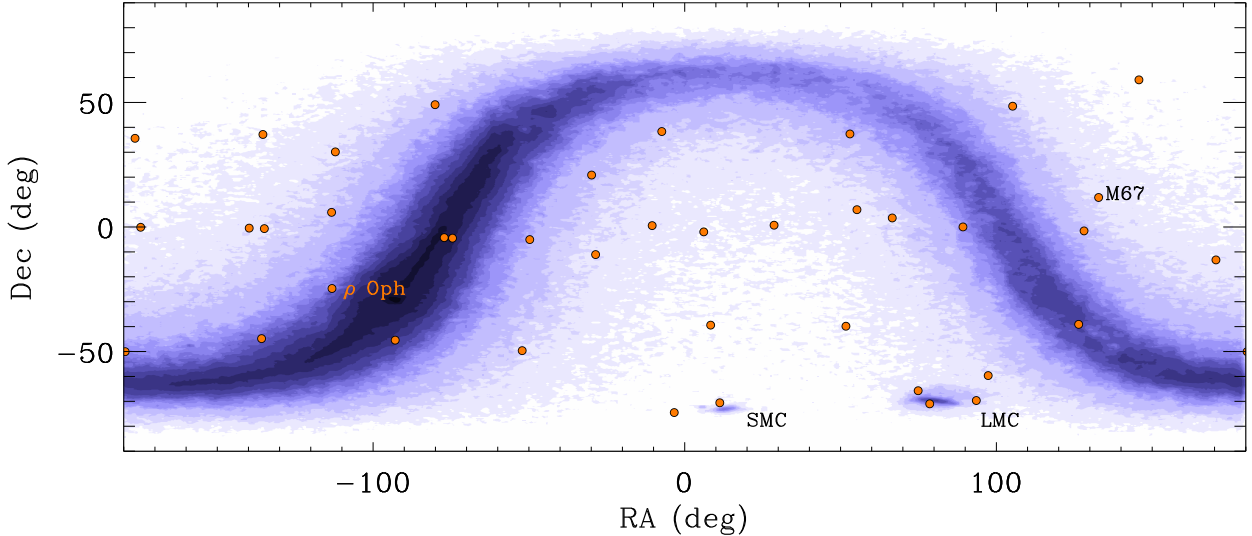


FIG. 1.— Spatial distribution of the 40 Cal-PSWDB tiles (orange circles), with titles for a few notable tiles labeled. Background contours denote increasing density from a sample of 3 million randomly drawn point sources from the 2MASS point source catalog, and trace the Galactic plane, bulge, and the Large and Small Magellanic Clouds.

bandpasses. Parks et al. (2013) have conducted a comprehensive study for variability of YSOs in the ρ Ophiuchus star forming region using the Cal-PSWDB light curves. Recently Quillen et al. (2014) have searched the Cal-PSWDB for red transient variables.

In this paper we present a census of the periodic variable objects from the time-domain calibration data. The data and period-finding methodology are outlined in §2. We describe the selection and classification of binary stars and radial pulsating objects in §3. Quasi-periodic and other large amplitude variables that were recovered are discussed in §4. We examine the general variability characteristics of point sources in the 2MASS calibration scans in §5, and concluding remarks are given in §6.

2. CAL-PSWDB DATA

The properties of the Cal-PSWDB survey have been extensively characterized in Plavchan et al. (2008b). We will briefly describe the survey, and outline our reanalysis of the light curves.

Each night during the main 2MASS survey, the two survey telescopes observed one of a series of calibration fields every hour with simultaneous JHK_s photometry. These calibration fields were observed with the same “freeze-frame” technique used in the entire 2MASS survey, and each calibration field visit produced a 7.8 second exposure. The raw calibration scan imaging was reduced and processed using the standard 2MASS data pipeline⁴.

A total of 35 calibration fields were observed, spread throughout the sky, with between 562 and 3692 epochs. During the final year of the 2MASS survey, five additional calibration fields were observed near the Large and Small Magellanic Clouds, which are included in our analysis of variable objects. The location of the 40 calibration fields are shown in Figure 1. The Cal-PSWDB contains in total over 196 million point source measurements from 74,772 scans of the 40 calibration fields.

We acquired the entirety of the Cal-PSWDB and LMC/SMC Cal-PSWDB through a bulk catalog download, and ingested all catalog data into a MySQL database. In these original data, the `gcntr` field was used as a unique identifier for all the merged point-source detections, i.e. all sources with the same `gcntr` should be associated with the same astrophysical object. However, the distributions of astrometric centroids for a significant number of these objects appeared multi-model, indicating insufficient object deblending at the catalog-level. For this reason, we performed a wholesale reanalysis of all of the point source positions, spatially clustering them into a final set of 113,030 “objects” using the OPTICS algorithm Ankerst et al. (1999).

For objects brighter than $J = 16$, the median number of J -band measurements per object increased from 432 to 671, while the median RMS of the astrometric centroids modestly decreased to $0.11''$ from $0.10''$ (when including objects fainter than $J = 16$, the median astrometric RMS decreased from $0.41''$ to $0.28''$). This indicates that OPTICS both performed a better job of deblending photometry of nearby objects, and at associating multiple epoch observations of the same object together.

Following this reclustering, bulk lightcurve metrics were calculated using only those data with photometric quality flags “A” through “C”, effectively limiting us to $S/N > 5$, and corrected photometric uncertainties smaller than 0.22 magnitudes. We calculated per-passband metrics including the error-weighted means and standard deviations, skew, kurtosis, a reduced χ^2 metric using all the data, and then a “robust” reduced χ^2_r metric excluding the brightest and faintest 10% of points. The χ^2_r metric will thus be less sensitive to single photometric outliers, but will also be less sensitive to periodic variables whose variability signal lasts a small fraction of its duty cycle, such as detached eclipsing binary stars.

⁴ <http://www.ipac.caltech.edu/2mass/releases/allsky/doc/explsup.html>

3. FINDING PERIODIC VARIABLES

To search for periodically variable objects, we used the **Supersmoothier** algorithm (Friedman 1984) that has been used in previous astronomical datamining applications (e.g. Becker et al. 2011). Data from each of the three passbands were folded and smoothed independently, resulting in three independent period estimates per object.

3.1. Selection Criteria

To select systems exhibiting periodic variability, we examined the periods returned in each of the three passbands. We applied two sets of criteria informed by previous multi-band periodic variability studies. Because **Supersmoothier** will report periods even when none are supported by the data, all stars in each candidate list were folded at their suggested periods, and visually inspected to verify the periodicity of the system, and to classify the sources.

The first selection criterion looks at the fractional uncertainty of the period estimates, similar to the analysis of Becker et al. (2011). Briefly, this requires that the standard deviation of the period estimates, or of the period estimates corrected for aliasing, are smaller than 10^{-4} of their average value. This criteria was applied using all 3 periods, and as a looser cut using only two of the three periods, since the K_S -band data typically have both lower signal-to-noise measurements and smaller lightcurve amplitudes. This cut yielded 2073 candidates, each of which were folded at the reported periods and validated through visual inspection. In total 157 systems from this list were verified as periodic systems.

As noted by Oluseyi et al. (2012), this may present too stringent of a cut for longer period systems. Because such systems will have gone through fewer oscillations in a given time window, their period is likely to be more poorly constrained. For this reason, we apply a second criterion, which requires that the standard deviation of the periods divided by their squared average is less than 10^{-5}day^{-1} . This set of cuts yielded 696 systems, of which 570 were new candidates (meaning it recovered 126/157 of the previous objects). **XXX** of these pass the human validation, and are included in this publication.

3.2. Visual Classification

Each of the **XXX** periodic systems was visually classified based upon its lightcurve shape, and best-fit period. These classifications were roughly based on four categories:

- Eclipsing binary stars: These lightcurves typically have two distinct minima corresponding to the primary and secondary eclipses of an edge-on binary system. These are further subdivided into detached and contact W UMa-type systems. The former have relatively flat out-of-eclipse lightcurve and sharp eclipse features, while the latter have more sinusoidal shapes and continuous variability. Contact systems may be confused with pulsating systems at half the period if the eclipse depths are similar.
- Pulsating variable stars: These lightcurves have a single minimum in their variability cycle, with an

overall sinusoidal lightcurve shape. Subclasses include Cepheids, RR Lyrae types RRab and RRc, and δ Scu objects. Subclassifications are made based upon period and lightcurve shape.

- Long period variables: These lightcurves typically have timescales of tens to hundreds of days. Lightcurve features do not exactly repeat, making period estimation difficult.
- Other: These lightcurve do not fit into any of the categories defined above. Two systems fall into this class, which are explored in further detail below.

4. ECLIPSING BINARY STARS

Our by-eye validation of periodic candidates yielded **XXX** binary stars.

match to new paper by Parks et al. (2013); Quillen et al. (2014)

to quantitatively separate these things, need a more impartial method. Eclipsing binaries and pulsating variables can be separated and classified by fitting Fourier modes to the light curves (Pojmanski 2002; Nefs et al. 2012). we used similar methods as other authors, using the IDL FOURFIT package by Buie (online CITE/footnote).

the binary type separation has been well-explored, and we use previously established equations (CITE Becker? for example). this puts them in 3 categories, which had excellent agreement with our initial by-eye analysis. we recover XX detached, YY semi-detached objects. contact binaries are called W UMa type, have very sinusoidal light curves. these are difficult to distinguish from rr lyr. sometimes they have color variations, but sometimes not if the mass ratio is near 1.

the separation between binary stars and rr lyrae is more difficult. some types of RR Lyr look very similar to binaries, most especially RR Lyr type a (CHECK ON THIS). to improve this, we need other types of Fourier cuts to quantify the asymmetry in the light curves. there is some previous work on this ((?)) but we found their cuts didn't make sense, possibly due to different fitting codes (?) or different wavelength(?)

using our by-eye categorization for objects, 8 for sure pulsators, we explored many combinations of Fourier parameter space. a_4/a_2 had been suggested previously as a good space to search in (Pojmanski 1997). b_1 makes sense, it is the first component of cosine asymmetry from the sinusoidal shape. binaries with eccentricity near 0 should not have any strong b modes.

To separate binaries from pulsators, we cut on:

$$b_1(\text{binary}) \geq -0.13 \left(\frac{a_4}{a_2} \right) - 0.3 \quad (1)$$

and different configurations of binaries can be determined using:

$$a_4(\text{detached}) \geq a_2(0.5 + a_2) \quad (2)$$

$$a_4(\text{contact}) \leq a_2(0.125 + a_2) \quad (3)$$

Using our by-hand classification, we can define the best line of delineation between contact and detached eclipsing binaries in this Fourier space. Rucinski (1997) used $a_4 < a_2(0.3 + a_2)$ to separate these two populations using

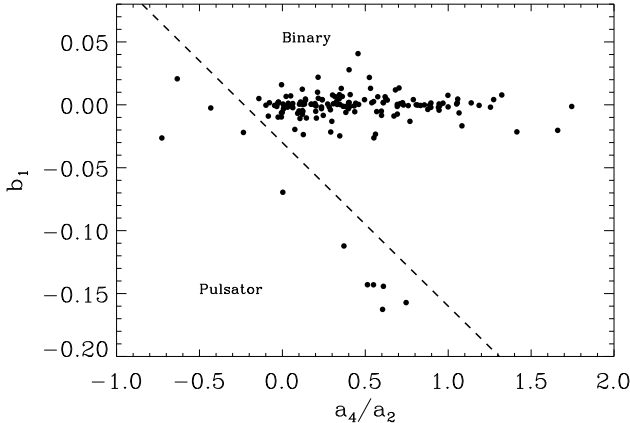


FIG. 2.— Fourier modes used to select between eclipsing binaries and pulsators (top) and different classes of eclipsing binaries (bottom).

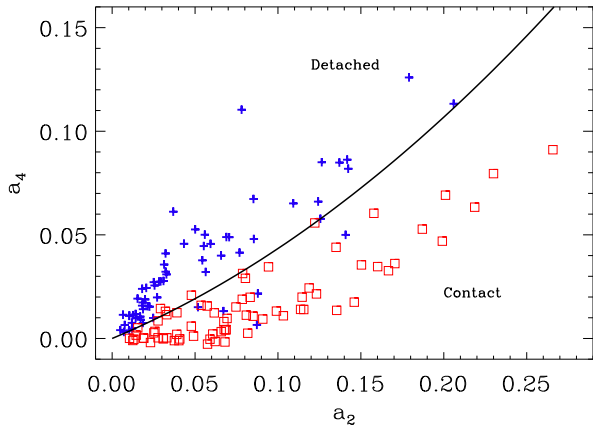


FIG. 3.— My classification of different classes of eclipsing binaries (bottom). separation given in text

OGLE light curves. We had 64 detached, 72 detached by hand classified. We used a brute-force approach to solve for the coefficient C in

$$a_4 = a_2(C + a_2), \quad (4)$$

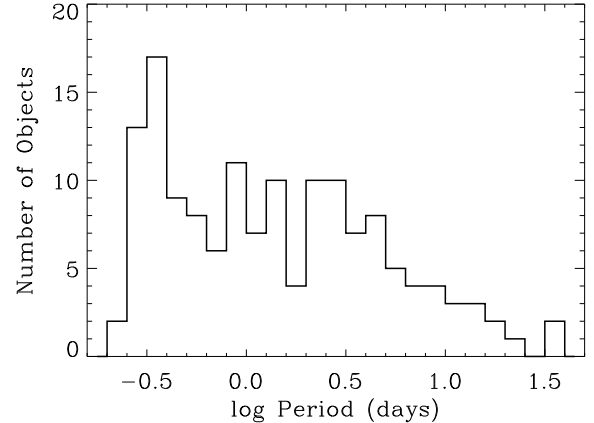


FIG. 4.— Distribution of periods for objects selected as binaries. Note the sharp cutoff at $\log P \sim -0.6$, $P \sim 0.25$ days.

calculating the fraction of each population correctly classified at each iteration. We used values of c ranging from 0 to 1, in steps of 0.001. The best degree of separation was found for $C = 0.334$, yielding 95% completeness for contact binaries, and 92% completeness for detached systems.

55 contact, 43 semi-detached, 48 detached binaries based on the equations

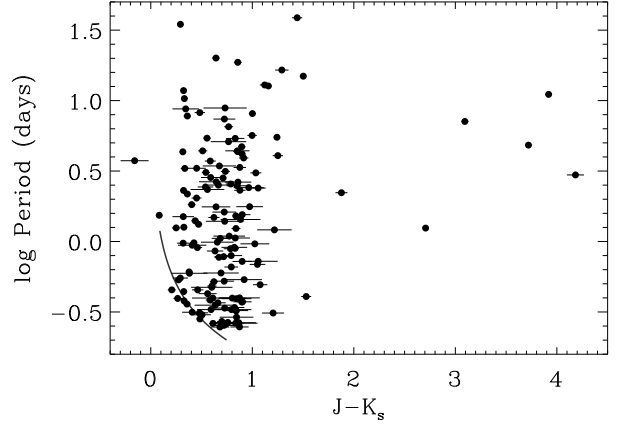


FIG. 5.— Period versus median colors for objects selected as binaries. The photometry was not corrected for reddening. The power law short period contact binary limit from Deb & Singh (2011) is shown for comparison (solid gray line). NEW COLOR FOR LINE, MAKE SYMBOLS DIFFERENT USING CLASSIFICATION FROM FIGURE 2/3

examples of each type

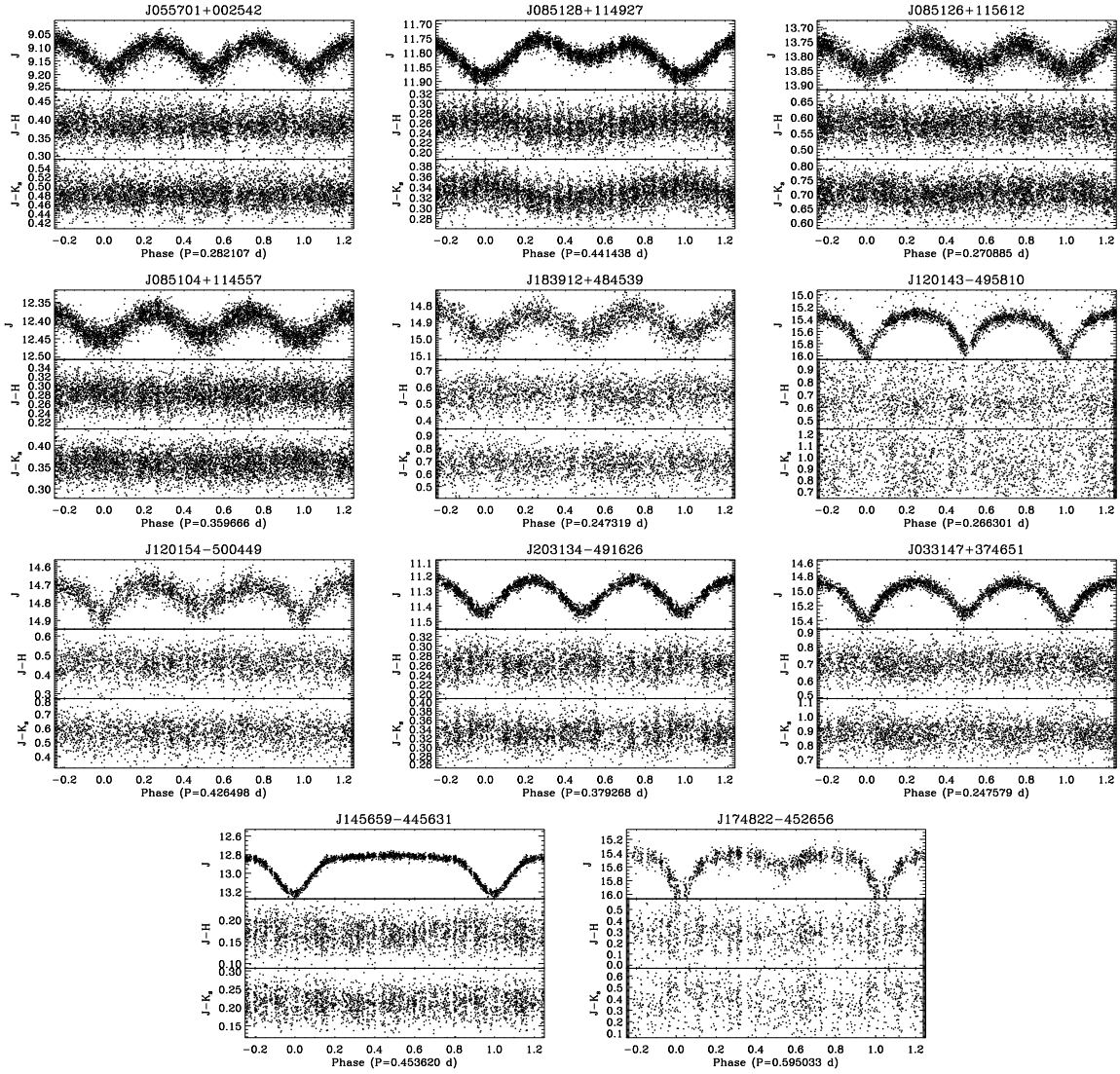


FIG. 6.— contact binaries

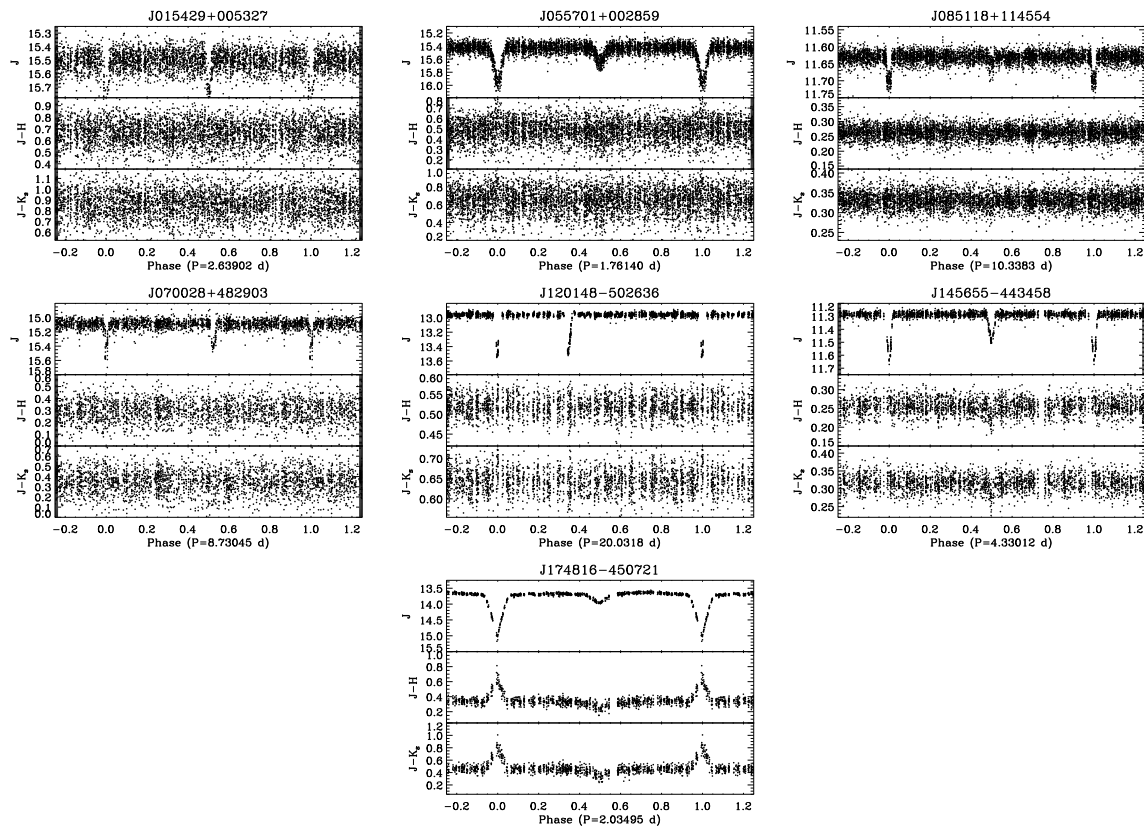


FIG. 7.— detached binaries

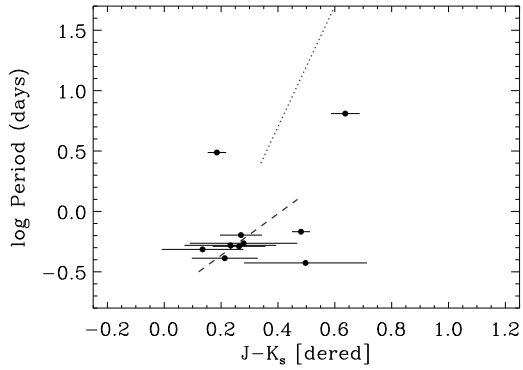


FIG. 8.— 17 radial pulsator variables. dashed line is theoretical prediction from Catelan et al. (2004) with $Z=0.001$ (no discernible dependence on Z) dotted line is for Cepheids, from ...

5. PULSATORS

Infrared observations of radial pulsating stars was first performed by Wisniewski & Johnson (1968), and detailed characterization was done for Cepheid variables by McGonegal et al. (1982) and for RR Lyr variables by Longmore et al. (1985)

K -band templates first derived in Jones et al. (1996)

RR Lyr type variables belong broadly to two classes: RRab and RRc, defined by their light curve morphologies (Bailey 1902)

Sollima et al. (2008) produced JHK_s light curves for the prototypical star, RR Lyr.

limited numbers found in the NIR, usually many few numbers of epochs and phase coverage (e.g. Del Principe et al. 2005)

– outline of section – these NIR light curves provide benchmarks for several classes of radial pulsating periodic variables. phase coverage is excellent for most of these objects

we have the best Cepheid NIR light curve, best regular RR Lyr, a good δ Scu, and probably some RR a and RR b types (need to look up difference). this list was matched up against SIMBAD, only XX were previously known about.

No Blazko variables - though should check the known sample to see if any have it and don't show it here.

the list is given in Table X, including distances computed using de-reddened and period-mag relations (CITE)

5.1. Effects of Shocks

the light curves can also be folded in to the color-mag space, and medians show kinks. we do this for all the objects.

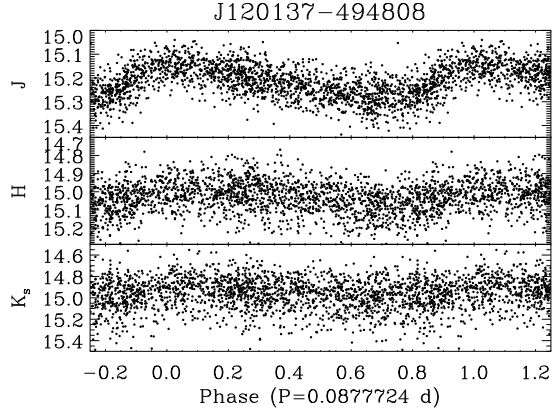


FIG. 9.— δ Scu variable

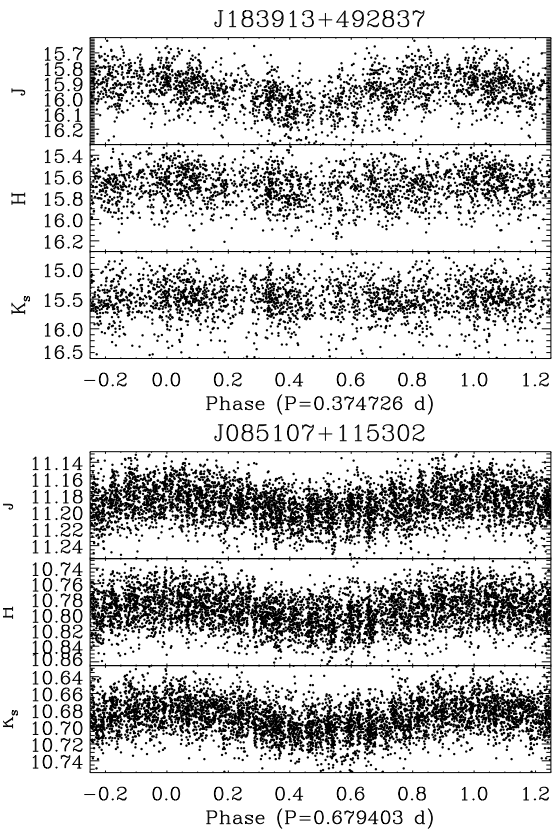


FIG. 10.— Pulsators with RRc-type light curves.

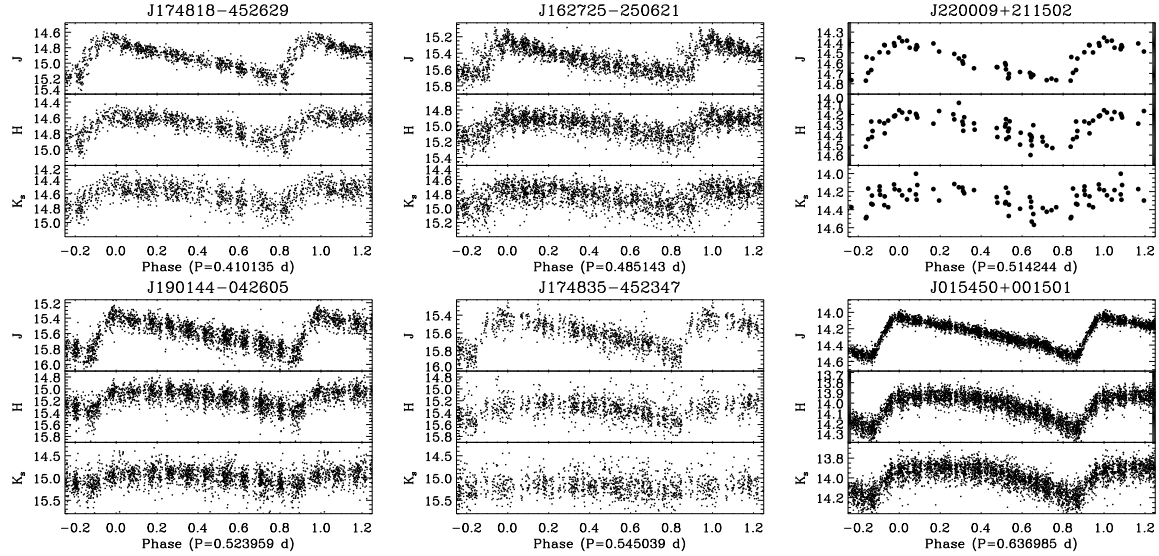


FIG. 11.— RRab-type variables

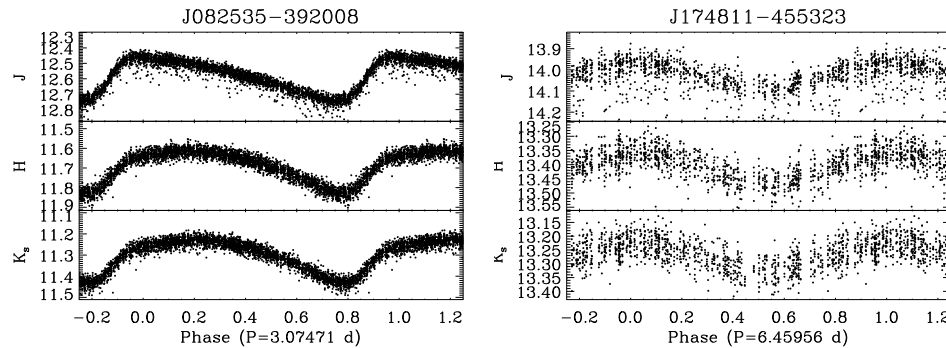


FIG. 12.— Pulsators (Cepheids) with periods longer than 2 days

6. NON-PERIODIC VARIABLES

Plavchan and student have done lots of work on this for ρ Oph field. We will only add other things that were identified by hand

7. AUTOMATED CLASSIFICATION

We next describe feature selection of the lightcurves and supervised learning of the boundaries between the different lightcurve classes. Feature selection requires reducing the time-series lightcurve to a set of numbers that summarize its behavior, such as period, amplitude, and skew. When initially approaching a problem, it is difficult to know *a priori* which features are most important for distinguishing one class of objects from another. Thus it is typical to select many features from the lightcurves, and to let the classifiers determine which are most important. Similar efforts have been described for optical lightcurves in the works of ?, ?, ?, and ?.

In an analysis of data from the LINEAR survey, ? use lightcurve period, amplitude, skew, and color as features for classification. As we have 3-band lightcurves, we construct colors from the median of the $J - H$ and $H - K$ lightcurves. We similarly use the instantaneous [W1-W2] colors from the WISE survey Wright et al. (2010), with the caveat that these are acquired at random phases in each lightcurve. Lightcurve skews are calculated using

the J , $J - H$, and $H - K$ lightcurves, and amplitudes are derived using the 5% to 95% measured range in J , $J - H$, and $H - K$. This yields 1 period, 3 colors, 3 amplitudes, and 3 skews as core lightcurve features.

Pojmanski (1997) find that by Fourier expanding lightcurves using the series:

$$m(\phi) = A_0 - \sum_{i=1}^4 A_i \cos(2\pi i\phi + \varphi) + B_i \sin(2\pi i\phi + \varphi)$$

the contact and detached binary systems may be separated out by looking at the distributions of A_4 vs. A_2 , and the pulsators may be separated from the contact systems by additionally looking at B_1 . This adds 3 additional features into our input set, yielding a total of 13.

8. CONCLUSIONS

The authors acknowledge support from NASA ADP grant NNX09AC77G.

This publication makes use of data products from the Two Micron All Sky Survey, which is a joint project of the University of Massachusetts and the Infrared Processing and Analysis Center/California Institute of Technology, funded by the National Aeronautics and Space Administration and the National Science Foundation.

REFERENCES

- Aihara, H., et al. 2011, ApJS, 193, 29
 Ankerst, M., Breunig, M. M., Kriegel, H.-P., & Sander, J. 1999, in SIGMOD 1999, Proceedings ACM SIGMOD International Conference on Management of Data, June 1-3, 1999, Philadelphia, Pennsylvania, USA, ed. A. Delis, C. Faloutsos, & S. Ghandeharizadeh (ACM Press), 49–60
 Bailey, S. I. 1902, Annals of Harvard College Observatory, 38, 1
 Becker, A. C., et al. 2008, MNRAS, 386, 416
 Becker, A. C., Bochanski, J. J., Hawley, S. L., Ivezić, Ž., Kowalski, A. F., Sesar, B., & West, A. A. 2011, ApJ, 731, 17
 Catelan, M., Pritzl, B. J., & Smith, H. A. 2004, ApJS, 154, 633
 Cutri, R. M. 2006, Explanatory Supplement to the 2MASS All Sky Data Release and Extended Mission Products, <http://www.ipac.caltech.edu/2mass/releases/allsky/doc/explsup.html>
 Davenport, J. R. A., Becker, A. C., Kowalski, A. F., Hawley, S. L., Schmidt, S. J., Hilton, E. J., Sesar, B., & Cutri, R. 2012, ApJ, 748, 58
 Deb, S., & Singh, H. P. 2011, MNRAS, 412, 1787
 Del Principe, M., Piersimoni, A. M., Bono, G., Di Paola, A., Dolci, M., & Marconi, M. 2005, AJ, 129, 2714
 Friedman, J. H. 1984, A Variable Span Smoother, Tech. Rep. 5, Department of Statistics, Stanford University
 Ivezić, Ž., et al. 2007, AJ, 134, 973
 Ivezić, Ž., et al. 2008, ArXiv e-prints, 0805.2366
 Jones, R. V., Carney, B. W., & Fulbright, J. P. 1996, PASP, 108, 877
 Kaiser, N., et al. 2002, in Society of Photo-Optical Instrumentation Engineers (SPIE) Conference Series, Vol. 4836, Survey and Other Telescope Technologies and Discoveries, ed. J. A. Tyson & S. Wolff, 154–164
 Longmore, A. J., Fernley, J. A., Jameson, R. F., Sherrington, M. R., & Frank, J. 1985, MNRAS, 216, 873
 McGonegal, R., McAlary, C. W., Madore, B. F., & McLaren, R. A. 1982, ApJ, 257, L33
 Nefs, S. V., et al. 2012, ArXiv e-prints, 1206.1200
 Nikolaev, S., Weinberg, M. D., Skrutskie, M. F., Cutri, R. M., Wheelock, S. L., Gizis, J. E., & Howard, E. M. 2000, AJ, 120, 3340
 Oluseyi, H. M., et al. 2012, AJ, 144, 9
 Parks, J. R., Plavchan, P., White, R. J., & Gee, A. H. 2013, ArXiv e-prints
 Plavchan, P., Gee, A. H., Stapelfeldt, K., & Becker, A. 2008a, ApJ, 684, L37
 Plavchan, P., Jura, M., Kirkpatrick, J. D., Cutri, R. M., & Gallagher, S. C. 2008b, ApJS, 175, 191
 Pojmanski, G. 1997, AcA, 47, 467
 —. 2002, AcA, 52, 397
 Quillen, A. C., Cioccia, M., Carlin, J. L., Meng, Z., & Bell, C. P. M. 2014, ArXiv e-prints
 Rucinski, S. M. 1997, AJ, 113, 1112
 Sarajedini, A., Dotter, A., & Kirkpatrick, A. 2009, ApJ, 698, 1872
 Sesar, B., Stuart, J. S., Ivezić, Ž., Morgan, D. P., Becker, A. C., & Woźniak, P. 2011, AJ, 142, 190
 Skrutskie, M. F., et al. 2006, AJ, 131, 1163
 Sollima, A., Cacciari, C., Arkharov, A. A. H., Larionov, V. M., Gorshanov, D. L., Efimova, N. V., & Piersimoni, A. 2008, MNRAS, 384, 1583
 Wisniewski, W. Z., & Johnson, H. L. 1968, Communications of the Lunar and Planetary Laboratory, 7, 57
 Wright, E. L., et al. 2010, AJ, 140, 1868

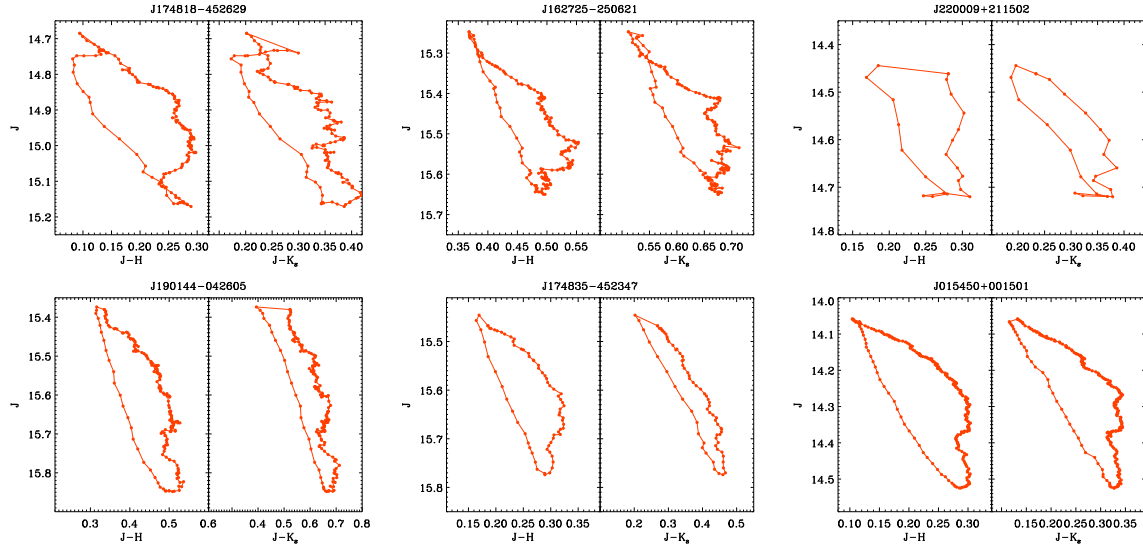


FIG. 13.— CMD of RRab pulsators

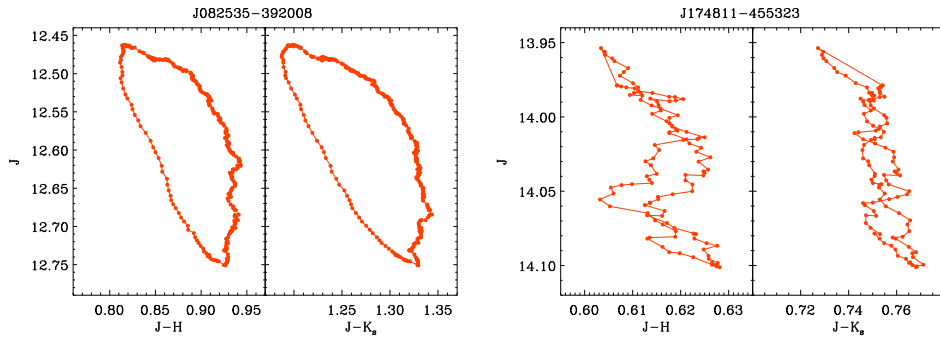


FIG. 14.— CMD of Pulsators (Cepheids) with periods longer than 2 days

TABLE 1
THE CATALOG OF QUASI-PERIODIC VARIABLES. (THIS TEX FILE NEEDS TO BE REVISED TO ONLY INCLUDE THE ACTUALLY INTERESTING OBJECTS, MOST ARE ALREADY SHOWN)

ObjectID (hhmmss+ddmmss)	FieldID	RA (deg)	Dec (deg)	$\langle J \rangle$ (mag)	$\langle H \rangle$ (mag)	$\langle K_s \rangle$ (mag)	# epochs	σ_J (mag)	σ_H (mag)	σ_K (mag)
J162659-243556	90009	246.74608	-24.59911	16.40	13.45	11.86	1543	0.01401	0.00569	0.00182
J162722-244807	90009	246.84578	-24.80195	10.92	9.83	9.34	1581	-0.00000	-0.00000	0.00046
J162718-245453	90009	246.82655	-24.91494	11.42	10.54	9.95	1567	0.07128	0.04564	0.02912

TABLE 2
THE CATALOG OF BINARY STARS, SELECTED USING FOURIER MODES. THE FULL VERSION OF THIS CATALOG (146 ENTRIES) WILL BE AVAILABLE ONLINE.

ObjectID (hhmmss+ddmmss)	FieldID	RA (deg)	Dec (deg)	Period (days)	$\langle J \rangle$ (mag)	$\langle H \rangle$ (mag)	$\langle K_s \rangle$ (mag)	# epochs	a_2	a_4	b_1
J015452+011053	90004	28.72067	1.18153	0.37205	13.62	12.94	12.72	2956	-0.00098	0.00166	0.01248
J015429+005327	90004	28.62207	0.89091	2.63902	15.51	14.84	14.65	2969	0.01922	-0.00187	0.01532
J162709-243408	90009	246.78799	-24.56892	4.83045	12.63	10.25	8.91	1580	0.03721	-0.00837	0.06224

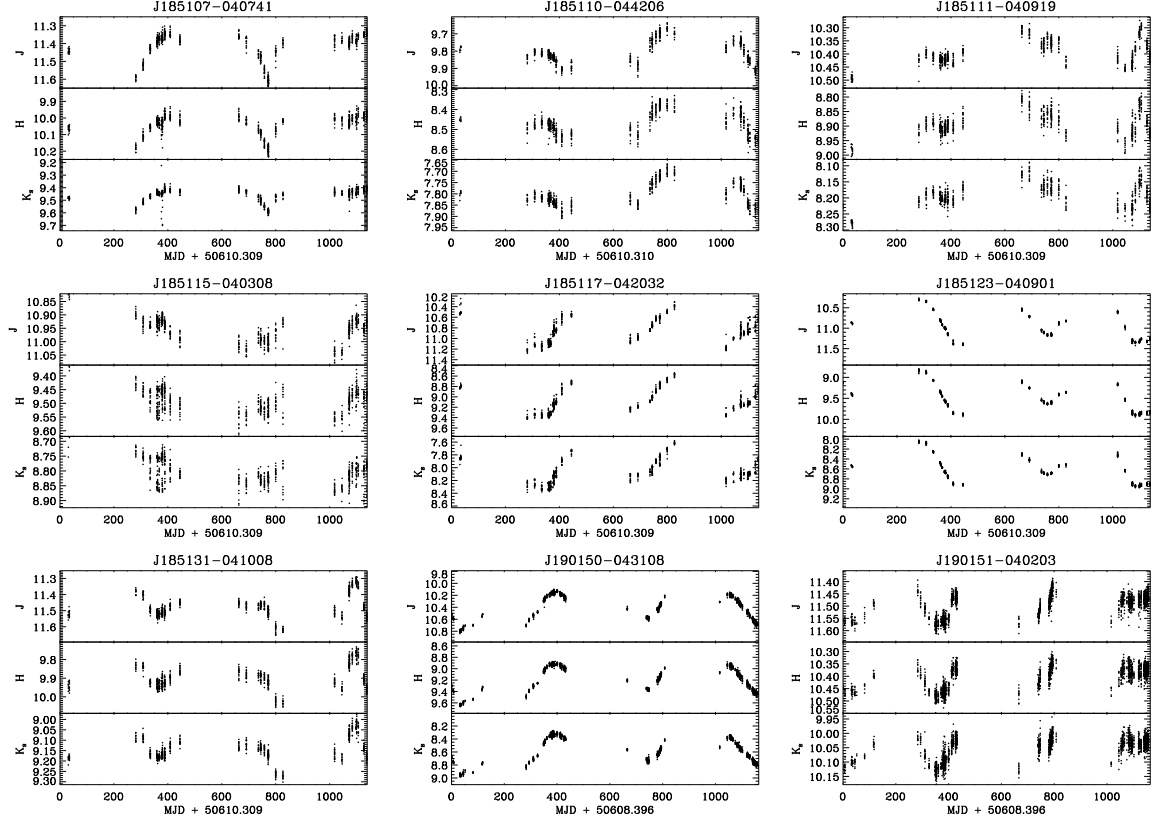


FIG. 15.— some long quasi-periodic variable objects. a couple look like DY Per's maybe? Nothing quite like RCB

TABLE 3
THE CATALOG OF RADIAL PULSATING TYPE PERIODIC VARIABLES, SELECTED USING FOURIER MODES.

ObjectID (hhmmss+ddmmss)	FieldID	RA (deg)	Dec (deg)	Period (days)	$\langle J \rangle$ (mag)	$\langle H \rangle$ (mag)	$\langle K_s \rangle$ (mag)	# epochs	a_2	a_4	b_1
J120137-494808	90217	180.40575	-49.80240	0.08777	15.22	15.03	14.95	1685	0.03441	-0.14304	0.06262
J183913+492837	90182	279.80688	49.47710	0.37473	15.96	15.68	15.43	1682	0.01161	-0.14297	0.02263
J174818-452629	90279	267.07571	-45.44157	0.41014	14.93	14.68	14.60	977	0.00012	-0.00248	-0.00028
J162725-250621	90009	246.85564	-25.10589	0.48514	15.46	14.98	14.82	1579	-0.00560	0.02069	0.00883
J220009+211502	92409	330.04028	21.25065	0.51424	14.60	14.35	14.29	41	-0.00234	-0.02196	0.00994
J190144-042605	90808	285.43744	-4.43475	0.52396	15.61	15.14	14.97	1879	-0.00112	-0.02633	0.00154
J174835-452347	90279	267.14786	-45.39640	0.54504	15.63	15.35	15.22	972	0.02224	-0.16258	0.03681
J015450+001501	90004	28.70900	0.25038	0.63698	14.27	14.01	13.98	2972	0.02093	-0.11219	0.05638
J085107+115302	90067	132.78021	11.88394	0.67940	11.19	10.80	10.69	3692	0.03375	-0.15717	0.04523
J082535-392008	90312	126.39848	-39.33574	3.07471	12.57	11.66	11.28	3501	0.00012	-0.06949	0.04578
J174811-455323	90279	267.04904	-45.88993	6.45956	14.02	13.40	13.27	968	0.03683	-0.14425	0.06046